RESEARCH ARTICLE

MASS EXTINCTION

On impact and volcanism across the Cretaceous-Paleogene boundary

Pincelli M. Hull[1]*†, André Bornemann[2]†, Donald E. Penman[1], Michael J. Henehan[1,3], Richard D. Norris[4], Paul A. Wilson[5], Peter Blum[6], Laia Alegret[7], Sietske J. Batenburg[8], Paul R. Bown[9], Timothy J. Bralower[10], Cecile Cournede[11,12], Alexander Deutsch[13], Barbara Donner[14], Oliver Friedrich[15], Sofie Jehle[16], Hojung Kim[9], Dick Kroon[17], Peter C. Lippert[18], Dominik Loroch[13], Iris Moebius[15,19], Kazuyoshi Moriya[20], Daniel J. Peppe[21], Gregory E. Ravizza[22], Ursula Röhl[14], Jonathan D. Schueth[23], Julio Sepúlveda[24], Philip F. Sexton[25], Elizabeth C. Sibert[4,26,27], Kasia K. Śliwińska[28], Roger E. Summons[29], Ellen Thomas[1,30], Thomas Westerhold[14], Jessica H. Whiteside[5], Tatsuhiko Yamaguchi[31], James C. Zachos[32]

The cause of the end-Cretaceous mass extinction is vigorously debated, owing to the occurrence of a very large bolide impact and flood basalt volcanism near the boundary. Disentangling their relative importance is complicated by uncertainty regarding kill mechanisms and the relative timing of volcanogenic outgassing, impact, and extinction. We used carbon cycle modeling and paleotemperature records to constrain the timing of volcanogenic outgassing. We found support for major outgassing beginning and ending distinctly before the impact, with only the impact coinciding with mass extinction and biologically amplified carbon cycle change. Our models show that these extinction-related carbon cycle changes would have allowed the ocean to absorb massive amounts of carbon dioxide, thus limiting the global warming otherwise expected from postextinction volcanism.

Sixty-six million years ago, two planetary-scale disturbances occurred within less than a million years of one another. One disturbance was the collision of an asteroid of more than 10 km in diameter with the Yucatan Peninsula at the boundary between the Cretaceous and the Paleogene [~66 million years ago (Ma)], producing the ~200-km-wide Chicxulub impact crater (*1*–*4*). Impact markers at hundreds of sites globally co-occur with the deposition of the Cretaceous-Paleogene (K/Pg) boundary clay and include elevated abundances of siderophilic elements such as iridium, osmium, and nickel, as well as tektites and shocked quartz (*1*, *5*, *6*). The other disturbance was the eruption of an estimated ~500,000 km^3 of lava across much of India and into the deep sea in a large igneous province known as the Deccan Traps (*7*, *8*) during the K/Pg boundary–spanning magnetochron C29r [65.688 to 66.398 Ma, ~710,000 years long (*9*)]. Deccan volcanism was, like most flood basalt eruptions (*8*, *10*, *11*), episodic, with flows deposited in pulses throughout magnetochron C29r (*12*, *13*). That both volcanism and the impact event occurred within several hundred thousand years of the K/Pg extinctions is beyond reasonable doubt (*5*, *8*, *12*, *13*). However, many aspects of the mass extinction event are still uncertain, including the relative timing and magnitude of volcanic effects on the biosphere (*13*, *14*), the potential relationship between impact and volcanism (*7*, *13*, *15*), and whether impact or volcanism acted as the sole, primary, or joint drivers of extinction (*5*, *10*, *16*).

The case for the Chicxulub impact as a driver of K/Pg mass extinction includes processes hypothesized to operate during the days and decades after the collision. The bolide impact injected an estimated >50,000 km^3 of ejecta (*4*), as well as ~325 billion metric tons (Gt) of sulfur and ~425 Gt of CO_2 and other volatiles (*17*) into the atmosphere from the marine carbonate and anhydrite target rock of the Yucatan Peninsula (*5*, *18*). The combined effects of an expanding impact fireball and the reentry of molten ejecta from the skies (*19*) may have raised temperatures to the point of spontaneous combustion near the impactor and caused severe heat stress and even death many thousands of kilometers away from the impact site in minutes to days after impact (*20*). In the days to years that followed, nitrogen and sulfur vapors reacted to form nitric and sulfuric acids and, with CO_2 gases, acidified the oceans (*21*–*23*). Finally, models and empirical evidence suggest that the combination of dust and aerosols precipitated a severe impact winter in the decades after impact (*24*–*27*).

Notable though these environmental effects may be, some researchers question whether the Chicxulub impactor acted as the sole or main driver of the K/Pg mass extinction for three primary reasons. First, no single kill mechanism appears to explain the extinction patterns: Acidification (*28*, *29*) and primary productivity decline (*30*) [due to darkness and cold (*26*)] are favored in the marine realm, whereas heat exposure and loss of productivity [due to fires, darkness, and cold (*18*, *26*)] are favored in the terrestrial realm (*31*, *32*). Second, asteroid and comet impacts have occurred throughout the history of life [although likely none the size and force of Chicxulub (*33*) have taken place in the past ~500 million years (Myr)], but no other mass extinction is unambiguously linked to such a collision (*34*). Third, flood basalt volcanism is strongly implicated as the driver of two of the most destructive mass extinctions in the last ~half-billion years [the Permian-Triassic (P/T) and Triassic-Jurassic (T/J) extinctions], leading some to favor a similar role for Deccan volcanism in the K/Pg mass extinction (*35*). However, most episodes of flood basalt volcanism after the T/J extinction produced no increase in extinction rates (*36*), potentially owing to substantial Earth system changes that dampened the effects of flood basalts after the P/T extinction.

Questions regarding the role of Deccan volcanism in driving the K/Pg mass extinction arise because of the relative lack of evidence

[1]Department of Geology and Geophysics, Yale University, New Haven, CT 06511, USA. [2]Bundesanstalt für Geowissenschaften und Rohstoffe, 30655 Hannover, Germany. [3]GFZ German Research Centre for Geosciences, 14473 Potsdam, Germany. [4]Scripps Institution of Oceanography, University of California San Diego, La Jolla, CA 92093, USA. [5]National Oceanography Centre Southampton, University of Southampton, Southampton SO14 3ZH, UK. [6]International Ocean Discovery Program, Texas A&M University, College Station, TX 77845, USA. [7]Departamento de Ciencias de la Tierra and Instituto Universitario de Ciencias Ambientales, Universidad Zaragoza, 50009 Zaragoza, Spain. [8]Géosciences Rennes, Université de Rennes 1, 35042 Rennes, France. [9]Department of Earth Sciences, University College London, London WC1E 6BT, UK. [10]Department of Geosciences, Pennsylvania State University, University Park, PA 16802, USA. [11]CEREGE, Université Aix-Marseille, 13545 Aix en Provence, France. [12]Institute for Rock Magnetism, University of Minnesota, Minneapolis, MN 55455, USA. [13]Institut für Planetologie, Universität Münster, 48149 Münster, Germany. [14]MARUM – Center for Marine Environmental Sciences, University of Bremen, 28359 Bremen, Germany. [15]Institute of Earth Sciences, Heidelberg University, 69120 Heidelberg, Germany. [16]Institut für Geophysik und Geologie, Universität Leipzig, 04103 Leipzig, Germany. [17]School of Geosciences, University of Edinburgh, Edinburgh EH8 9XP, UK. [18]Department of Geology & Geophysics, The University of Utah, Salt Lake City, UT 84112, USA. [19]Department of Biogeochemical Systems, Max Planck Institute for Biogeochemistry, 07745 Jena, Germany. [20]Department of Earth Sciences, Waseda University, Shinjyuku-ku, Tokyo 169-8050, Japan. [21]Department of Geosciences, Baylor University, Waco, TX 76798, USA. [22]Department of Earth Sciences, University of Hawai'i at Mānoa, Honolulu, HI 96822, USA. [23]ConocoPhillips Company, Houston, TX 77079, USA. [24]Department of Geological Sciences and Institute of Arctic and Alpine Research, University of Colorado Boulder, Boulder, CO 80309, USA. [25]School of Environment, Earth and Ecosystem Sciences, The Open University, Milton Keynes MK7 6AA, UK. [26]Harvard Society of Fellows, Harvard University, Cambridge, MA 02138, USA. [27]Department of Earth and Planetary Sciences, Harvard University, Cambridge, MA 02138, USA. [28]Department of Stratigraphy, Geological Survey of Denmark and Greenland (GEUS), DK-1350 Copenhagen K, Denmark. [29]Department of Earth, Atmospheric and Planetary Sciences, Massachusetts Institute of Technology, Cambridge, MA 02139, USA. [30]Department of Earth and Environmental Sciences, Wesleyan University, Middletown, CT 06459, USA. [31]National Museum of Nature and Science, Tsukuba, 305-0005, Japan. [32]Department of Earth and Planetary Sciences, University of California, Santa Cruz, CA 95064, USA.
*Corresponding author. Email: pincelli.hull@yale.edu †These authors contributed equally to this work.

for a volcanogenic driver. Despite advances in chronology, the timing of the most voluminous Deccan eruptions relative to the K/Pg extinctions remains unclear (*7*, *8*). In earlier studies, many researchers argued that most Deccan flood basalts (>85%) were emplaced in a relatively short interval before the K/Pg, starting around the C29r/C30n boundary (~66.39 Ma) and ending well before the K/Pg impact (*11*, *12*). In contrast, Renne *et al.* (*13*) and Sprain *et al.* (*8*) proposed that the vast majority of Deccan basalts were emplaced after the impact. Schoene *et al.* (*7*) largely agree with the basalt flow ages of Sprain *et al.* and Renne *et al.* (*8*, *13*) but place the K/Pg boundary higher in the lava pile (i.e., in the upper part of, or above, the Poladpur Formation) and therefore propose major pulses of emplacement immediately before and immediately after the impact (*7*).

Pre- and postimpact scenarios are debated in part because they are tied to different environmental disruption scenarios. Pre-event volcanism may have acted in concert with the impact to drive K/Pg extinctions (*10*), whereas post-event volcanism suggests a role for volcanism in the delayed recovery of biodiversity (*13*). For the environment and life, the main environmental effects of large igneous provinces are attributed to volatile release (*37*–*39*), not lava emplacement, and the magnitude of volcanic outgassing is not necessarily linked directly to the volume of erupted lava. If early eruptive phases of flood basalt volcanism have higher volatile concentrations, then most volatiles could have been released before the impact, even if most of the lava was emplaced afterward (*8*).

Here we provide constraints on Deccan Trap outgassing by comparing well-resolved and temporally detailed ocean drilling and global temperature records, with five modeled end-member scenarios for the timing, magnitude, and composition of outgassing (*40*). These comparisons allow us to consider the relative effects of Deccan Trap outgassing and bolide impact on the marine carbon cycle and biological change.

Marine environmental record of outgassing

Deccan Trap degassing released a mix of volatiles including SO_2, Cl and other halogens, and CO_2, with sulfur having perhaps the greatest direct effect on ecosystems through acidification and pronounced global cooling (>4.5°C) (*38*). However, the environmental effects of SO_2 would have been relatively short-lived (years to centuries at most) and difficult to detect in slowly accumulating deep-sea sediments. In contrast, the influence of CO_2 emissions should be clearly evident in marine sediments as a global warming event paired with a carbon isotope anomaly (*41*). We used this diagnostic fingerprint of CO_2 emissions as a proxy for the timing of potentially disruptive outgassing of sulfur (and other noxious gases) and to test which volcanic degassing scenarios are compatible with the observed record.

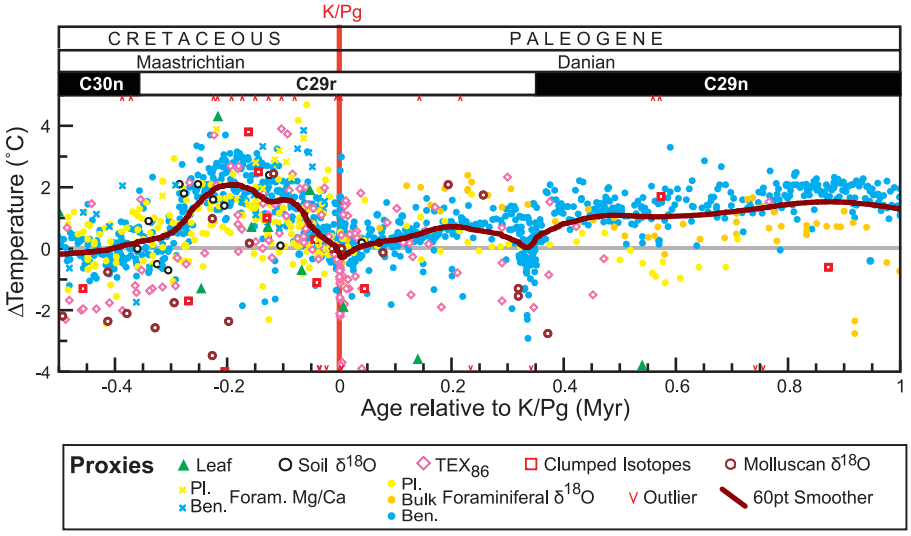

Fig. 1. Global temperature change across the K/Pg boundary. New and existing empirical temperature records from marine sediments (foraminiferal $\delta^{18}O$, foraminiferal Mg/Ca, and TEX_{86} measurements), shallow marine carbonates (clumped isotopes of mollusk carbonate), and terrestrial proxies (leaf margin analysis, biomarkers, clumped isotopes of mollusk carbonate) were aligned to a common age model (tables S2 and S3) and normalized to the latest Cretaceous temperature within each record. A 60-point fast Fourier transform (FFT) smoother of global temperature change is shown in dark red. Data are provided in tables S4 to S12. Some outlying data points do not fall within plot bounds but can be seen in figs. S1 to S16. Pl., planktonic; Ben., benthic; Foram., foraminiferal.

Two dominant features are clear in our global temperature compilation (Fig. 1) (*40*). First, marine and terrestrial records show a late Maastrichtian warming event of ~2°C, on average (figs. S1 to S16) (*42*–*44*), in the Cretaceous part of C29r that cooled back to pre-event temperatures before the K/Pg boundary (Fig. 1). Second, temperatures in the earliest Danian were comparable to those in the late Maastrichtian before the warming event, with temperatures gradually increasing to become >1°C warmer, on average, by ~600 thousand years (kyr) after the impact. Benthic foraminiferal oxygen isotope records, which typically track changes in global mean temperatures, show both of these features (Figs. 1 and 2 and fig. S13A), as do most other archives (figs. S1 to S16). The two exceptions, the bulk carbonate records and fish teeth phosphate records from El Kef (figs. S10C, S11, and S12), likely do not track global temperature for extinction-related reasons (*40*) and thus were excluded from our calculation of global mean temperatures.

Our multiproxy, astronomically tuned record from the North Atlantic site (*45*) has an especially complete Maastrichtian sequence and a millimeter-thick tektite layer at the K/Pg boundary (Fig. 2 and figs. S17 to S19). The record documents an excursion to lower $\delta^{13}C$ values in bulk sediments, coincident with $\delta^{18}O$ decline (a warming indicator) as well as a decline in osmium isotope values (Fig. 2 and figs. S20 and S21). Similar patterns are noted in records from the South Atlantic Walvis Ridge and the North Pacific Shatsky Rise (Fig. 2 and figs. S18 and S19) (*42*, *46*). The similarity of these records across three such widespread localities and four sites (Fig. 2) suggests that they provide a largely complete record of magnetochron C29r. Slight temporal offsets in the apparent onset and recovery from the latest Maastrichtian warming (among all sites) and in early Paleogene carbon isotope patterns at Shatsky Rise, due to short unconformities and/or the limitations of cyclostratigraphic age models, illustrate the current temporal uncertainties (Fig. 2). Temperature and atmospheric CO_2, as reflected in both our $\delta^{18}O$ and $\delta^{13}C$ anomalies and recent boron isotope records (*23*), returned to prewarming values in the very latest Maastrichtian. The most prominent feature in the records is the pronounced decline in $\delta^{13}C$ isotopes and change in sedimentary $CaCO_3$ content beginning at the K/Pg boundary (Fig. 2).

We investigated the timing of Deccan Trap outgassing by modeling the effects of CO_2 and sulfur emissions on long-term global temperatures using the geochemical box model LOSCAR (Long-term Ocean Sediment CArbon Reservoir v. 2.0.4) (*47*). Guided by published hypotheses for the timing and volume of trap emplacement, we tested five major Deccan Trap emission scenarios differing in the timing of volatile release: (i) case 1 (leading), with

the majority (87%) of degassing taking place before the K/Pg boundary [after (*10*)]; (ii) case 2 (50:50), with half of the degassing occurring before and half after the K/Pg boundary [after the lower estimate in (*8*)]; (iii) case 3 (punctuated), with four pulses including a major event just preceding the K/Pg boundary [after (*7*)]; (iv) case 4 (lagging), with the majority (87%) of degassing taking place after the K/Pg boundary [inverse case 1 pre- and post-outgassing volumes (*13*)]; and (v) case 5 (spanning), with emissions released evenly throughout magnetochron C29r [after (*12*)] (Table 1). All volcanic outgassing scenarios assume the same (i) initial climatic and oceanographic conditions [600 parts per million P_{CO_2} (partial pressure of CO_2) and climate sensitivity of 2° to 4°C per CO_2 doubling (*41*), LOSCAR's Paleogene ocean configuration and circulation, and marine [Mg^{2+}] of 42 mmol/kg and [Ca^{2+}] of 21 mmol/kg], (ii) K/Pg impact volatile release from the target rock (325 Gt S; 425 Gt CO_2) (*17*), (iii) upper and lower estimates for total volcanic outgassing volumes [4091 to 9545 Gt C and 3200 to 8500 Gt S (*10*) at constant ratios] (*40*), and (iv) extinction-related changes in the marine carbon cycle (*41*, *48*) (including reductions in both organic carbon and carbonate export and increases in intermediate-depth organic carbon remineralization; see Table 1) that taper back to pre-event values over 1.77 Myr after the extinction (*49*). In most outgassing scenarios, we assumed a common onset of Deccan degassing at the C30n/C29r boundary, following geochronology of the traps (*7*, *8*, *12*, *50*). In the age framework used to align the temperature records [i.e., GTS 2012 (*9*)], the C30n/C29r boundary is 358 kyr before the K/Pg boundary rather than the ~250 to 300 kyr indicated by the most recent $^{40}Ar/^{39}Ar$ and U-Pb geochronology (*7*, *50*). Simulations were initially tuned (*40*) to find the biological scenario (iv) that minimized mismatches between the data and model (figs. S22 to S27), and multiple scenarios for climate sensitivity and outgassing were considered in assessing goodness of fit (Figs. 3 and 4, figs. S25 and S28 to S32, and Table 2).

Three modeled scenarios differ distinctly from the observed pattern of temperature change (Fig. 3), and we thus consider them unlikely to represent the true outgassing history. Case 3 fails to reproduce the late Maastrichtian warming and shows a pronounced boundary-crossing warming event that is not supported by proxy data. In case 4, late Maastrichtian warming is too muted and early Paleocene warming is too pronounced, and in case 5 warming increases up to the K/Pg boundary, unlike in the empirical record (Fig. 3). Relatively poor model fit is also indicated by high mean

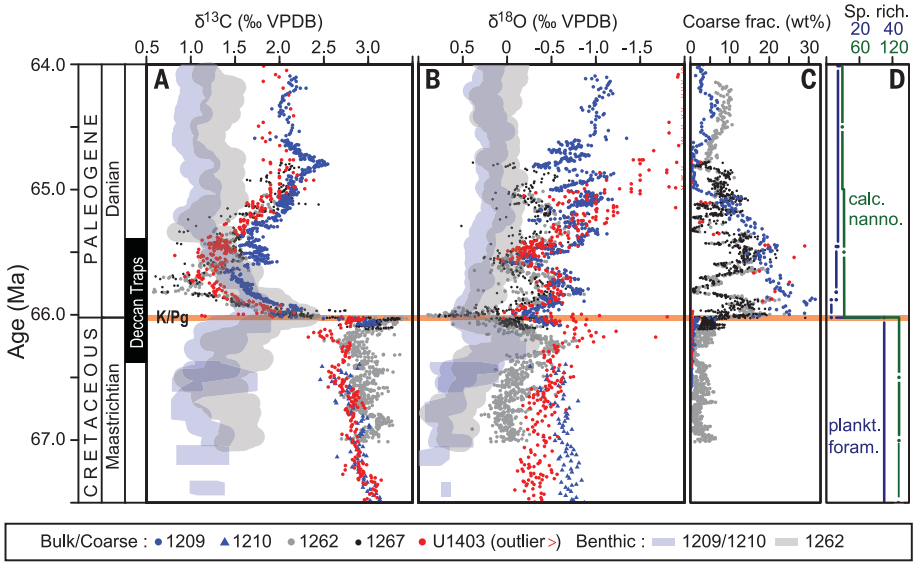

Fig. 2. K/Pg boundary dynamics at the best-resolved deep-sea sites globally: Shatsky Rise, Walvis Ridge, and J-Anomaly Ridge. High-resolution (**A**) carbon and (**B**) oxygen isotope dynamics in benthic foraminifera (transparent shaded areas) and bulk carbonate (discrete points) and (**C**) sediment composition (weight % coarse fraction) at Shatsky Rise (blue), Walvis Ridge (gray), and J-Anomaly Ridge (red). (**D**) Global records of nannofossil (green) and foraminifera [blue, from (*61*)] species richness (*40*). The major interval of Deccan Trap emplacement (estimated 93% of volume) is indicated at left by the black bar (*8*). Ocean drilling sites are listed by number. VPDB, Vienna Pee Dee belemnite; calc. nanno., calcareous nannofossil; plankt. foram., planktonic foraminifera; Sp. rich., species richness.

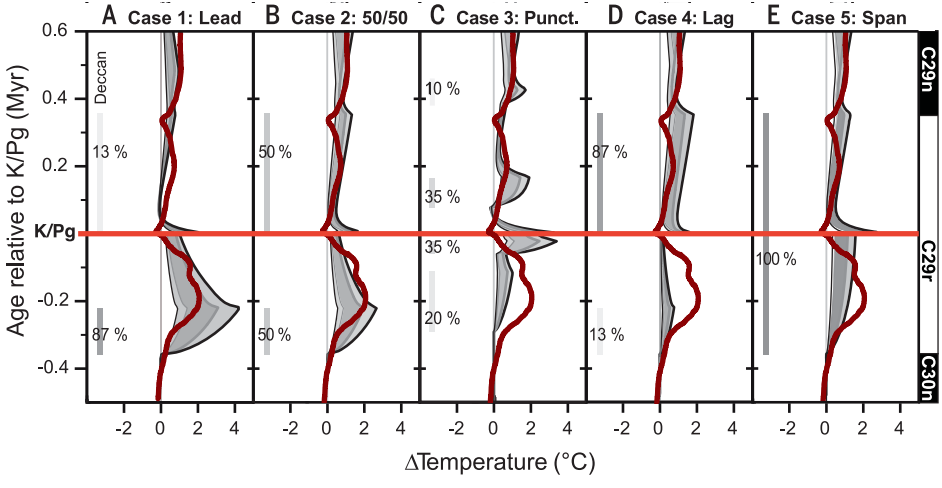

Fig. 3. Global temperature change across the K/Pg boundary compared to modeled temperature change in five scenarios for Deccan Trap outgassing. Outgassing scenarios include (**A**) case 1 (leading), with most outgassing before impact; (**B**) case 2 (50:50), with 50% outgassing before impact and 50% after impact; (**C**) case 3 (punctuated), with four pulses including a major event just before the K/Pg boundary; (**D**) case 4 (lagging), with most outgassing after impact; and (**E**) case 5 (spanning), with continuous outgassing throughout magnetochron C29r (Table 1). Each model scenario is represented by four lines (bounding a shaded region) delineating different combinations of climate sensitivity and volcanic outgassing: high degassing (9545 Gt C and 8500 Gt S) and 3°C per CO_2 doubling (thick gray line); high degassing and 4°C per doubling (thick black line); low degassing (4090 Gt C and 3200 Gt S) and 3°C per doubling (thin gray line); and low degassing and 2°C per doubling (thin black line). A 60-point FFT smoother of global temperature change (red line; see Fig. 1) is provided for comparison. The timing of Deccan outgassing assumed in each scenario is indicated by the bars at left in each panel, with the shading intensity of the bar denoting the proportion of outgassing in that interval.

absolute errors (MAEs) for cases 3 and 4 as compared with cases 1 and 2 (Table 2). The temporal dynamics of $\delta^{13}C$ in cases 3 and 5 also deviates from the empirical record (Fig. 4).

Only two outgassing scenarios produce modeled temperatures resembling those of the empirical records: the leading case (case 1) and the 50:50 case (case 2). We thus consider these the two most likely of the tested scenarios to represent Deccan Trap outgassing. In case 1, most CO_2 and SO_2 degassing occurred in the latest Maastrichtian, leading to global warming and subsequent cooling before the K/Pg. The relatively constant early Paleocene temperatures of case 1, with a gradual warming over the 600 kyr after the impact, are also consistent with empirical records (Figs. 1 to 3 and figs. S17 to S18). Case 2 (50:50) also matches the empirical temperature record well (Fig. 3), with the lowest MAEs of all cases (Table 2). The Late Cretaceous warming differs between case 1 and case 2 because of the reduced Late Cretaceous volcanic outgassing in the latter. Although uncertainty about climate sensitivity (*51*) and total Deccan Trap emissions (*10*, *12*) has a greater effect on modeled temperatures than the difference in outgassing volume between case 1 and case 2 (Fig. 3 and figs. S25 and S28), carbon isotopes also support case 2 as the more likely scenario (Fig. 4; see also MAEs in table S31).

The climatic effects of a major pulse (50%) of Deccan outgassing released over the ~350 kyr

Table 1. Model parameters for five focal Deccan outgassing scenarios tested in LOSCAR. Δ denotes change in value (reduction or increase). pre, before impact; post, after impact; Frac. int.-depth C_{org} remin., fraction of intermediate depth organic carbon remineralization.

	Case 1: Leading	Case 2: 50:50	Case 3: Punctuated	Case 4: Lagging	Case 5: Spanning
			Volcanic outgassing		
Pulse 1 (pre): Volume	87% of total high: 8305 Gt C, 7395 Gt S low: 3559 Gt C, 2784 Gt S	50% of total high: 4773 Gt C, 4250 Gt S low: 2045 Gt C, 1600 Gt S	20% of total high: 1909 Gt C, 1700 Gt S low: 818 Gt C, 640 Gt S	13% of total high: 1241 Gt C, 1105 Gt S low: 532 Gt C, 416 Gt S	100% of total high: 9545 Gt C, 8500 Gt S low: 4091 Gt C, 3200 Gt S
Timing	Starts: −358 kyr Ends: −218 kyr	Starts: −358 kyr Ends: −218 kyr	Starts: −290 kyr Ends: −110 kyr	Starts: −358 kyr Ends: −218 kyr	Starts: −358 kyr Ends: 355 kyr
Pulse 2 (pre): Volume			35% of total high: 3340 Gt C, 2975 Gt S low: 1431 Gt C, 1120 Gt S		
Timing			Starts: −60 kyr Ends: −20 kyr		
Pulse 1 (post): Volume	13% of total high: 1241 Gt C, 1105 Gt S low: 532 Gt C, 416 Gt S	50% of total high: 4773 Gt C, 4250 Gt S low: 2045 Gt C, 1600 Gt S	35% of total high: 3340 Gt C, 2975 Gt S low: 1431 Gt C, 1120 Gt S	87% of total high: 8305 Gt C, 7395 Gt S low: 3559 Gt C, 2784 Gt S	
Timing	Starts: 0 kyr Ends: 355 kyr	Starts: 0 kyr Ends: 355 kyr	Starts: 80 kyr Ends: 170 kyr	Starts: 0 kyr Ends: 355 kyr	
Pulse 2 (post): Volume			10% of total high: 955 Gt C, 850 Gt S low: 409 Gt C, 320 Gt S		
Timing			Starts: 390 kyr Ends: 430 kyr		
			Impact outgassing		
Volume	100% of total 115 Gt C, 325 Gt S	100% of total 115 Gt C, 325 Gt S	100% of total 115 Gt C, 325 Gt S	100% of total 115 Gt C, 325 Gt S	100% of total 115 Gt C, 325 Gt S
Timing	Starts: 0 kyr Ends: 1 kyr	Starts: 0 kyr Ends: 1 kyr	Starts: 0 kyr Ends: 1 kyr	Starts: 0 kyr Ends: 1 kyr	Starts: 0 kyr Ends: 1 kyr
			Biotic change		
Organic export flux Δ	50% reduction	50% reduction	50% reduction	50% reduction	50% reduction
$CaCO_3$ export flux Δ	42.5% reduction	42.5% reduction	42.5% reduction	42.5% reduction	42.5% reduction
Frac. int.-depth C_{org} remin. Δ	22% increase	22% increase	22% increase	22% increase	22% increase
Timing	Starts: 0 kyr immediately tapers Ends: 1770 kyr	Starts: 0 kyr immediately tapers Ends: 1770 kyr	Starts: 0 kyr immediately tapers Ends: 1770 kyr	Starts: 0 kyr immediately tapers Ends: 1770 kyr	Starts: 0 kyr immediately tapers Ends: 1770 kyr

immediately after the impact (case 2) were limited by extinction-related changes to the carbon cycle, including the reduction in $CaCO_3$ export from pelagic calcifiers to the seafloor. Marine $CaCO_3$ export indirectly affects atmospheric CO_2 by changing the distribution of carbon and alkalinity between the surface and the deep ocean and slows the removal of alkalinity from the system via $CaCO_3$ burial (*41*). The difference between cases 1 and 2 is almost imperceptible, with case 2 having slightly warmer (~0.25°C) early Danian temperatures than case 1. Notably, more-rapid Paleocene outgassing, such as that modeled in case 3 [after (*7*)], exceeds the capacity of the altered marine carbon cycle to absorb CO_2.

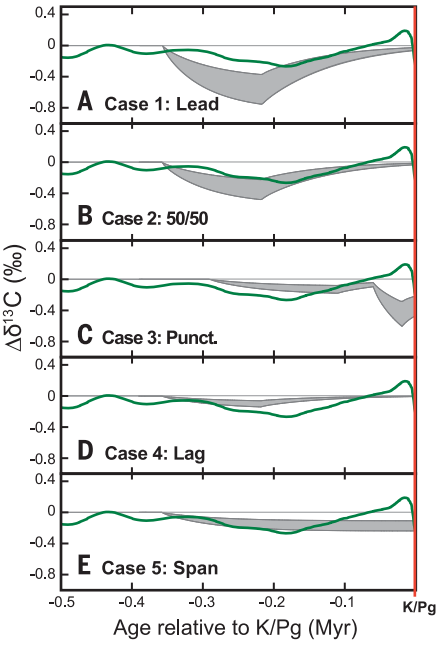

Fig. 4. Surface ocean $\delta^{13}C$ change across the late Maastrichtian warming compared to modeled $\delta^{13}C$ change in five scenarios for Deccan Trap outgassing. (**A** to **E**) Bulk carbonate $\Delta\delta^{13}C$ (20-point FFT smoother of data from Site U1403 and Site 1262) is shown against surface ocean $\delta^{13}C$ for end-member outgassing and climate sensitivity scenarios (gray shaded area) for each case, as detailed in Fig. 3. In each case, carbonate carbon isotopes are expressed as $\Delta\delta^{13}C$, relative to the late Maastrichtian high of 3.03‰ at 0.432 Myr before the onset of the CO_2 release (see also figs. S36 and S37).

Our results inform several boundary debates. First, if there was a large pulse of emplacement 20 to 60 kyr before the impact (*7*), then most CO_2 outgassing (and associated environmental impacts) must have preceded lava emplacement by several hundred thousand years. This would be before the eruption of the most voluminous stages of Deccan volcanism (i.e., before the Wai subgroup), as modeled for cases 1 and 2 [Figs. 3 and 4; see expanded discussion in (*40*)]. Second, roughly equal pre- and postimpact volcanic degassing is supported (case 2; Figs. 3 and 4), a hypothesized scenario in (*8*). However, our results are not consistent with most (>75%) volcanogenic degassing after impact [i.e., outgassing more similar to other eruptive volumes in (*8*, *13*)], because modeled warming is too muted in the Cretaceous and too pronounced in the early Paleocene (case 4) as compared with empirical records (Fig. 3). Third, impact-related volatile release from the target rock has a negligible climatic effect (fig. S24) and thus is unlikely to account for the pronounced warming in the first 100 kyr indicated by fish teeth $\delta^{18}O$ records (*52*). Instead, this record likely predominantly reflects changes in fish biology rather than temperature. Fourth, biotic recovery can account for the apparently gradual early Danian warming, as observed in marine records, if it begins at or shortly after impact and occurs over >1.5 Myr. This biotic recovery scenario reproduces the general pattern of change in $\delta^{13}C$ gradients (Fig. 2 and fig. S27), carbonate saturation state (Fig. 2C and fig. S27), and temperature but differs from recovery hypotheses that posit a delay in the onset of biological recovery for ~500 kyr or more (*40*, *49*, *53*).

No marine evidence for joint cause in mass extinction

The fossil record indicates no lasting, outsized, or cascading effect of the late Maastrichtian warming event on marine ecosystems of the sort that might predispose them to mass extinction by impact. First, we found no evidence for elevated extinction rates in the latest Cretaceous in marine taxa (table S1), excepting a contested record from Seymour Island, Antarctica (*54*, *55*). The scarcity of biostratigraphic datums in the Cretaceous portion of magnetochron C29r signifies a conspicuous lack of extinction in geographically widespread species, including planktonic foraminifera, nannoplankton, radiolarians, and ammonites (*9*). Second, late Cretaceous outgassing did not have a lasting effect on the community structure of well-fossilized taxa. Although range and community shifts coincided with warming, a shift back to the prewarming-like communities occurred before impact (table S1). Third, marine carbon cycle indicators ($\delta^{13}C$ and carbonate deposition) show no discernable effect of late Maastrichtian outgassing and warming on a major ecosystem function: the export and cycling of carbon. The $\delta^{13}C$ anomaly size [~0.2 to 0.3 per mil (‰); see also (*44*)] is consistent with a volcanogenic driver as in case 2 (Figs. 2 and 4 and fig. S28) given the magnitude of warming, without biological amplification.

In contrast, major and enduring changes to ecosystems coincided with the K/Pg impact. In deep-sea records, impact markers occur at the level of the abrupt mass extinction of >90% of planktonic foraminifera and 93% of nannoplankton species (Fig. 2). These groups exhibit rapid turnover and high dominance in community composition in the first 500 kyr of the Paleocene (*56*, *57*), when bulk carbonate $\delta^{18}O$ likely reflects community composition rather than surface ocean temperatures (Fig. 5 and

Table 2. Mean absolute error (MAE) and mean minimum absolute error (MMAE) of cases relative to the interpolated global temperature record. MMAE was calculated for each case by determining whether the empirical data fell outside of the temperature range bounded by the high- and low-outgassing scenarios, given a climate sensitivity of 3°C per CO_2 doubling, and, if so, by how much. MAEs were also calculated for each outgassing volume and climate sensitivity shown in Fig. 3. MMAEs and MAEs were calculated on a 20-kyr interpolated time step from 360 kyr before and 600 kyr after the K/Pg. Case 2 consistently has the lowest MAEs, and cases 1 and 2 have the lowest MMAEs. volc., volcanic outgassing; doub., doubling.

	MMAE	MAE (high volc., 3°C per CO_2 doub.)	MAE (high volc., 4°C per CO_2 doub.)	MAE (low volc., 3°C per CO_2 doub.)	MAE (low volc., 2°C per CO_2 doub.)
Case 1	0.25	0.46	0.65	0.50	0.58
Case 2	0.21	0.35	0.43	0.48	0.58
Case 3	0.45	0.59	0.65	0.58	0.64
Case 4	0.45	0.61	0.69	0.56	0.63
Case 5	0.29	0.40	0.44	0.53	0.61

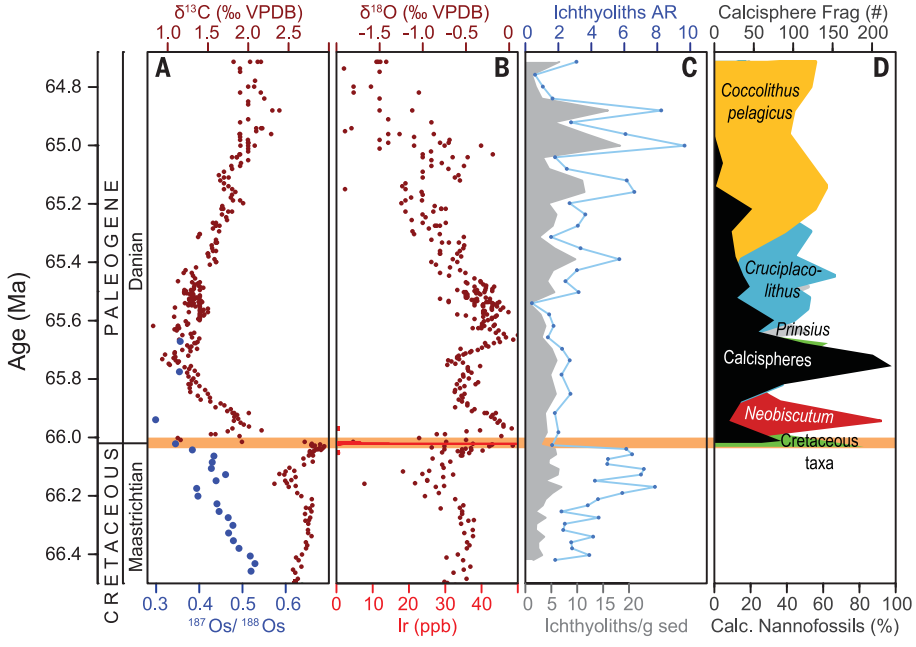

Fig. 5. Late Cretaceous warming and early Paleocene record of environmental and biotic change at IODP Site U1403, J-Anomaly Ridge, Newfoundland. A negative carbon isotope anomaly (**A**) coincides with late Cretaceous warming in $\delta^{18}O$ (**B**) and osmium isotope evidence for volcanism (A) at IODP Site U1403. The collapse in surface ocean $\delta^{13}C$ values (A) coincides with an iridium anomaly (B) and step change in fish tooth accumulation (**C**). The earliest Paleocene $\delta^{18}O$ values of bulk carbonate appear to be strongly influenced by vital effects driven by rapid turnover in the dominant calcareous nannofossil taxa (**D**) in sites globally (figs. S18, S34, and S35). Data are in tables S12, S16, S17, and S29. AR, accumulation rate; Frag, fragment; ppb, parts per billion; sed, sediment.

figs. S33 to S35). At the same time, tracers of the marine carbon cycle indicate a profound change in marine ecosystem function. The community structure of some groups, such as small fishes, which show no evidence of elevated extinction, changed permanently (*58*). The $\delta^{13}C$ composition of planktonic foraminifera and nannoplankton fell to or below that of benthic foraminifera at the iridium anomaly (Figs. 2 and 5 and figs. S34 and S35) (*43*, *49*). The loss or inversion of the $\delta^{13}C$ gradient typically maintained by the biological pump is unmatched in the fossil record of pelagic calcifiers (~170 Myr) and indicates that the K/Pg boundary impact had an outsized effect on the marine carbon cycle.

After the impact, an already-altered marine carbon cycle would have been needed to counteract the CO_2 emitted by a major postimpact pulse of outgassing, as in case 2 (Fig. 3), to avoid a warming event of the same magnitude as the Late Cretaceous warming event. This suggests that the major ecological change of the K/Pg mass extinction must have occurred before any major postimpact volcanism. Our modeling supports a scenario in which Deccan volcanism could have contributed to the aftermath of the impact and mass extinction, as in (*13*), if environmentally destructive gases such as SO_2, halogens, or sulfate aerosols contributed to (or drove) the persistence of unusual marine communities for the first ~500 kyr of the Paleocene. This might be particularly true if the evolution of the magma chamber led to higher sulfur content of later emissions, as in other eruption types (*59*). However, no observations document acidification coupled to extreme cold snaps in the earliest Paleocene, as predicted by this hypothesis, and there is no explanation for why SO_2 would have greater biotic effects in the well-buffered early Danian oceans than in the latest Maastrichtian oceans (figs. S1 to S18).

Outlook

We combined climatic, biotic, and carbon cycle records with modeled impact and outgassing scenarios and found support for a bolide impact as the primary driver of the end-Cretaceous mass extinction. Our analysis suggests that ~50% of Deccan Trap CO_2 outgassing occurred well before the impact, but it does not support the suggestion (*7*) that a large outgassing event took place a mere ~10 to 60 kyr before impact. This suggests a pronounced decoupling between CO_2 outgassing and lava flow emplacement, if the conclusions of Schoene *et al.* (*7*) are correct. Alternatively, our results support a relative impact and eruption chronology similar to the findings of Sprain *et al.* (*8*) and our best-supported, 50:50 outgassing scenario. The Late Cretaceous warming event attributed to Deccan degassing is of a comparable size to small warming events in the Paleocene and early Eocene that are not associated with elevated extinction or turnover (*43*, *60*), similar to what we find for the late Maastrichtian. We therefore conclude that impact and extinction created the initial opportunity for the rise of Cenozoic species and communities, but Deccan volcanism might have contributed to shaping them during the extinction aftermath.

REFERENCES AND NOTES

1. L. W. Alvarez, W. Alvarez, F. Asaro, H. V. Michel, *Science* **208**, 1095–1108 (1980).
2. A. R. Hildebrand *et al.*, *Geology* **19**, 867–871 (1991).
3. B. Collen *et al.*, *Biol. Lett.* **12**, 20150843 (2016).
4. J. Morgan *et al.*, *Nature* **390**, 472–476 (1997).
5. P. Schulte *et al.*, *Science* **327**, 1214–1218 (2010).
6. G. Ravizza, D. VonderHaar, *Paleoceanography* **27**, PA3219 (2012).
7. B. Schoene *et al.*, *Science* **363**, 862–866 (2019).
8. C. J. Sprain *et al.*, *Science* **363**, 866–870 (2019).
9. F. M. Gradstein, J. G. Ogg, M. D. Schmitz, G. M. Ogg, Eds., *The Geologic Time Scale 2012* (Elsevier, 2012).
10. A. L. Chenet *et al.*, *J. Geophys. Res.* **114**, B06103 (2009).
11. A. L. Chenet, X. Quidelleur, F. Fluteau, V. Courtillot, S. Bajpai, *Earth Planet. Sci. Lett.* **263**, 1–15 (2007).
12. B. Schoene *et al.*, *Science* **347**, 182–184 (2015).
13. P. R. Renne *et al.*, *Science* **350**, 76–78 (2015).
14. P. R. Renne *et al.*, *Science* **339**, 684–687 (2013).
15. M. A. Richards *et al.*, *Geol. Soc. Am. Bull.* **127**, 1507–1520 (2015).
16. E. Font *et al.*, *Earth Planet. Sci. Lett.* **484**, 53–66 (2018).
17. N. Artemieva, J. Morgan; Expedition 364 Science Party, *Geophys. Res. Lett.* **44**, 10180–10188 (2017).
18. S. P. S. Gulick *et al.*, *Proc. Natl. Acad. Sci. U.S.A.* **116**, 19342–19351 (2019).
19. D. A. Kring, D. D. Durda, *J. Geophys. Res.* **107**, 5062 (2002).
20. J. Morgan, N. Artemieva, T. Goldin, *J. Geophys. Res. Biogeosci.* **118**, 1508–1520 (2013).
21. S. Ohno *et al.*, *Nat. Geosci.* **7**, 279–282 (2014).
22. T. Tyrrell, A. Merico, D. I. Armstrong McKay, *Proc. Natl. Acad. Sci. U.S.A.* **112**, 6556–6561 (2015).
23. M. J. Henehan *et al.*, *Proc. Natl. Acad. Sci. U.S.A.* **116**, 22500–22504 (2019).
24. J. Vellekoop *et al.*, *Proc. Natl. Acad. Sci. U.S.A.* **111**, 7537–7541 (2014).
25. K. Kaiho *et al.*, *Sci. Rep.* **6**, 28427 (2016).
26. J. Brugger, G. Feulner, S. Petri, *Geophys. Res. Lett.* **44**, 419–427 (2017).
27. C. G. Bardeen, R. R. Garcia, O. B. Toon, A. J. Conley, *Proc. Natl. Acad. Sci. U.S.A.* **114**, E7415–E7424 (2017).
28. L. Alegret, E. Thomas, K. C. Lohmann, *Proc. Natl. Acad. Sci. U.S.A.* **109**, 728–732 (2012).
29. B. J. Marshall, R. C. Thunell, M. J. Henehan, Y. Astor, K. E. Wejnert, *Paleoceanography* **28**, 363–376 (2013).
30. M. Aberhan, S. Weidemeyer, W. Kiessling, R. A. Scasso, F. A. Medina, *Geology* **35**, 227–230 (2007).
31. P. M. Sheehan, T. A. Hansen, *Geology* **14**, 868–870 (1986).
32. D. S. Robertson, M. C. McKenna, O. B. Toon, S. Hope, J. A. Lillegraven, *Geol. Soc. Am. Bull.* **116**, 760–768 (2004).
33. E. M. Shoemaker, *J. R. Astron. Soc. Can.* **92**, 297–309 (1998).
34. J. D. Archibald *et al.*, *Science* **328**, 973 (2010).
35. G. Keller, J. Punekar, P. Mateo, *Palaeogeogr. Palaeoclimatol. Palaeoecol.* **441**, 137–151 (2016).
36. S. V. Sobolev *et al.*, *Nature* **477**, 312–316 (2011).
37. M. T. Jones, D. A. Jerram, H. H. Svensen, C. Grove, *Palaeogeogr. Palaeoclimatol. Palaeoecol.* **441**, 4–21 (2016).
38. A. Schmidt *et al.*, *Nat. Geosci.* **9**, 77–82 (2016).
39. S. Self, S. Blake, K. Sharma, M. Widdowson, S. Sephton, *Science* **319**, 1654–1657 (2008).
40. Materials and methods are available as supplementary materials.
41. M. J. Henehan, P. M. Hull, D. E. Penman, J. W. B. Rae, D. N. Schmidt, *Philos. Trans. R. Soc. B* **371**, 20150510 (2016).
42. J. S. K. Barnet *et al.*, *Geology* **46**, 147–150 (2018).
43. J. S. K. Barnet *et al.*, *Paleoceanogr. Paleoclimatol.* **34**, 672–691 (2019).

44. L. Q. Li, G. Keller, *Geology* **26**, 995–998 (1998).
45. R. D. Norris, P. A. Wilson, P. Blum, Expedition 342 Scientists, in *Proc. IODP, 342*, R. D. Norris, P. A. Wilson, P. Blum, Expedition 342 Scientists, Eds. (Integrated Ocean Drilling Program, 2014); http://publications.iodp.org/proceedings/342/342toc.htm.
46. N. Robinson, G. Ravizza, R. Coccioni, B. Peucker-Ehrenbrink, R. Norris, *Earth Planet. Sci. Lett.* **281**, 159–168 (2009).
47. R. E. Zeebe, *Geosci. Model Dev.* **5**, 149–166 (2012).
48. J. C. Zachos, M. A. Arthur, W. E. Dean, *Nature* **337**, 61–64 (1989).
49. H. S. Birch, H. K. Coxall, P. N. Pearson, D. Kroon, D. N. Schmidt, *Geology* **44**, 287–290 (2016).
50. C. J. Sprain, P. R. Renne, W. A. Clemens, G. P. Wilson, *Geol. Soc. Am. Bull.* **130**, 1615–1644 (2018).
51. E. J. Rohling *et al*., *Annu. Rev. Mar. Sci.* **10**, 261–288 (2018).
52. K. G. MacLeod, P. C. Quinton, J. Sepúlveda, M. H. Negra, *Science* **360**, 1467–1469 (2018).
53. S. D'Hondt, P. Donaghay, J. C. Zachos, D. Luttenberg, M. Lindinger, *Science* **282**, 276–279 (1998).
54. J. D. Witts *et al*., *Nat. Commun.* **7**, 11738 (2016).
55. T. S. Tobin, *Sci. Rep.* **7**, 16317 (2017).
56. P. M. Hull, R. D. Norris, T. J. Bralower, J. D. Schueth, *Nat. Geosci.* **4**, 856–860 (2011).
57. J. J. Pospichal, in *The Cretaceous-Tertiary Event and Other Catastrophes in Earth History*, G. Ryder, D. E. Fastovsky, S. Gartner, Eds. (GSA Special Paper 307, Geological Society of America, 1996), pp. 335–360.
58. E. C. Sibert, M. Friedman, P. M. Hull, G. Hunt, R. D. Norris, *Proc. R. Soc. B* **285**, 20181194 (2018).
59. M. Edmonds, *Philos. Trans. R. Soc. London Ser. A* **366**, 4559–4579 (2008).
60. P. F. Sexton *et al*., *Nature* **471**, 349–352 (2011).
61. R. D. Norris, in *Palaeobiology II*, D. E. G. Briggs, P. G. Crowther, Eds. (Blackwell Science, 2001), pp. 229–231.

ACKNOWLEDGMENTS

This research used samples and/or data provided by the International Ocean Discovery Program (IODP), which was sponsored by the U.S. National Science Foundation and participating countries under management of Joint Oceanographic Institutions, Inc., and its predecessors—the (Integrated) Ocean Drilling Program and the Deep Sea Drilling Program. We thank the *JOIDES Resolution* crew of IODP Expedition 342 and W. Hale and A. Wuelbers for help with sampling. We also thank the many centers and staff scientists who enabled the measurements, including L. Elder in the Hull laboratory (Yale University), B. Erkkila and M. Wint at the Yale Analytical and Stable Isotope Center, D. Andreasen at the UCSC Stable Isotope Laboratory, and F. Demory (CEREGE) for help with magnetic data production and processing. This work benefited from helpful discussions with J. Dinarès-Turell, the insights of C. B. Keller, and the comments of four anonymous reviewers. **Funding:** IODP USSSP Post-Expedition Activity award and Yale University support to P.M.H.; Deutsche Forschungsgemeinschaft (DFG) funding (grants BO2505/8-1 and EH 89/20-2) to A.B.; Yale Peabody Museum support to M.J.H.; Spanish Ministry of Economy and Competitiveness and FEDER funds (CGL2017-84693-R) to L.A.; DFG funding (grant VO687/14) to S.J.B.; a Richard Foster Flint Postdoctoral Fellowship (Department of Geology and Geophysics, Yale University) to D.E.P.; DFG funding (grant number FR2544/2) to O.F.; NSF funding (EAR-132552) and American Chemical Society Petroleum Research Fund (grant PRF#52822-DN18) to D.J.P.; DFG funding (grants RO1113/3, RO1113/4, and RO1113/8) to U.R.; the NASA Exobiology Program (grant NNX09AM88G) to R.E.S.; the Danish Council for Independent Research/Natural Sciences (DFF/FNU) (grant 11-107497) to K.K.Ś.; NSF funding (OCE 1536611) to E.T.; DFG funding (grant WE5479/3) to T.W.; and a NERC (NE/K006800/1) and Royal Society Wolfson award to P.A.W. **Author contributions:** P.M.H. conceived and co-led the study, drafted the manuscript, contributed to model design, generated empirical data, and edited data tables and figures. A.B. co-led the study; coordinated data generation, reporting, figures, and tables; generated empirical data; and substantially contributed to study design and text. D.E.P. led LOSCAR modeling and substantially contributed to study design and text. M.J.H. compiled and aligned age models for the global temperature compilation, prepared related tables and figures, and substantially contributed to study design and text. R.D.N., P.A.W, and P.B. led IODP Expedition 342, with R.D.N. and P.A.W. substantially contributing to study design and text. L.A., S.J.B., P.R.B., T.J.B., C.C., A.D., B.D., O.F., S.J., H.K., D.K., P.C.L., D.L., I.M., K.M., D.J.P., G.E.R., U.R., J.S., J.D.S., E.C.S., K.K.Ś., R.E.S., E.T., T.W., J.H.W., and T.Y. contributed empirical datasets, figures, and related analyses, interpretations, and text. L.A., P.R.B., T.J.B., O.F., D.K., P.F.S., J.S., E.T., T.W., J.H.W., and J.C.Z. substantially contributed to ideas and/or text. All authors read and approved the final text. The primary contribution of R.D.N., P.A.W., P.B., S.J.B., P.R.B., C.C., A.D., O.F., S.J., H.K., P.C.L., D.L., I.M., K.M., G.E.R., U.R., J.S., P.F.S., E.C.S., K.K.Ś., R.E.S., T.W., J.H.W., and T.Y. was the IODP Expedition 342 K/Pg boundary investigation. In the byline, the first seven authors appear in order of contribution; all others are listed alphabetically.
Competing interests: The authors have no competing interests.
Data and materials availability: All data are available in the manuscript and the supplementary materials.

SUPPLEMENTARY MATERIALS

science.sciencemag.org/content/367/6475/266/suppl/DC1
Materials and Methods
Supplementary Text
Figs. S1 to S44
Tables S1 to S31
References

24 June 2019; accepted 5 December 2019
10.1126/science.aay5055

On impact and volcanism across the Cretaceous-Paleogene boundary

Pincelli M. Hull, André Bornemann, Donald E. Penman, Michael J. Henehan, Richard D. Norris, Paul A. Wilson, Peter Blum, Laia Alegret, Sietske J. Batenburg, Paul R. Bown, Timothy J. Bralower, Cecile Cournede, Alexander Deutsch, Barbara Donner, Oliver Friedrich, Sofie Jehle, Hojung Kim, Dick Kroon, Peter C. Lippert, Dominik Loroch, Iris Moebius, Kazuyoshi Moriya, Daniel J. Peppe, Gregory E. Ravizza, Ursula Röhl, Jonathan D. Schueth, Julio Sepúlveda, Philip F. Sexton, Elizabeth C. Sibert, Kasia K. Sliwinska, Roger E. Summons, Ellen Thomas, Thomas Westerhold, Jessica H. Whiteside, Tatsuhiko Yamaguchi and James C. Zachos

Science **367** (6475), 266-272.
DOI: 10.1126/science.aay5055

An impact with a dash of volcanism

Around the time of the end-Cretaceous mass extinction that wiped out dinosaurs, there was both a bolide impact and a large amount of volcanism. Hull *et al.* ran several temperature simulations based on different volcanic outgassing scenarios and compared them with temperature records across the extinction event. The best model fits to the data required most outgassing to occur before the impact. When combined with other lines of evidence, these models support an impact-driven extinction. However, volcanic gases may have played a role in shaping the rise of different species after the extinction event.

Science, this issue p. 266